Mechanical Systems and Signal Processing 127 (2019) 290–305

Contents lists available at ScienceDirect

Mechanical Systems and Signal Processing

journal homepage: www.elsevier.com/locate/ymssp

Pole placement in uncertain dynamic systems by variance minimisation

L.J. Adamson *, S. Fichera, B. Mokrani, J.E. Mottershead

School of Engineering, University of Liverpool, Liverpool L69 3GH, United Kingdom

ARTICLE INFO

Article history:
Received 8 October 2018
Received in revised form 22 January 2019
Accepted 3 March 2019

Keywords:
Receptance method
Optimal pole placement
Structural dynamics
Uncertainty quantification

ABSTRACT

The problem of pole placement in dynamic systems with uncertainties is addressed using a global optimisation approach. Variability between nominally identical systems, which arises from manufacturing tolerances, wear and environmental variability, is considered. In the proposed method, receptances are measured from one of the open-loop, nominal systems chosen at random. In this case, in addition to the variability about the parameter means, the parameter means are also random. The receptance method is then used to place the poles of the measured system such that their spread, due to parameter uncertainty, is minimised. The measure used to assess the spread is the variance, determined efficiently by a polynomial chaos expansion. Among the advantages of the method are: (i) there is no requirement to model the system since experimental receptances are used, (ii) it is not necessary to measure the mean system, and (iii) uncertainty in poles is quantified across its full range by using variances. Numerical and experimental examples are provided to illustrate the working of the proposed method.

1. Introduction

Manufacturing variability, unknown environmental conditions and random degradation cause uncertainty in structural parameters [1], which results in variability in measured natural frequencies and damping. Conventional analysis techniques, such as the finite-element method (FEM), are usually deterministic and therefore do not explicitly consider the effects of uncertainty. Moreover, such techniques usually assume average structural parameters, which are estimated [2]. As a consequence, there may exist a high degree of discrepancy between predicted and experimentally obtained parameters. It is desired, therefore, that alternative analysis techniques that quantify and reduce the effects of uncertainty are used.

Robust design optimisation (RDO) and reliability-based design optimisation (RBDO) have been used in recent years to address this problem. In both methods, an objective function that weights both performance and robustness criteria is defined such that the system achieves optimum performance with minimal compromise to its robustness or probability of failure [3]. In the context of dynamic systems, the conventional approach is to passively modify structural elements such that the overall stiffness and damping of the system is changed in some desirable way. An alternative approach is to actively modify the system using feedback control. By assigning closed-loop poles, the frequency and damping of some, or all, of a system's poles can be altered [4]. This is known as pole placement.

* Corresponding author.
E-mail addresses: l.j.adamson@liverpool.ac.uk (L.J. Adamson), sebastiano.fichera@liverpool.ac.uk (S. Fichera), b.mokrani@liverpool.ac.uk (B. Mokrani), j.e.mottershead@liverpool.ac.uk (J.E. Mottershead).

https://doi.org/10.1016/j.ymssp.2019.03.007
0888-3270/

Nomenclature

a_i	polynomial chaos weighting constants
$\mathbf{b}$	force distribution vector
$\mathbf{C}$	stiffness matrix
$\mathbf{f}, \mathbf{g}$	control gains
$\mathbf{H}$	receptance matrix
$\mathbf{H}_m$	measured receptance matrix
$\mathbf{K}$	stiffness matrix
$\mathbf{M}$	mass matrix
s	complex variable
$\mathbf{x}$	vector of degrees-of-freedom
y	random function
$\mathbf{Z}$	dynamic stiffness matrix
$\bar{\mathbf{Z}}$	mean dynamic stiffness matrix
$\tilde{\mathbf{Z}}$	random dynamic stiffness contribution matrix
$\mathbf{Z}_m$	measured dynamic stiffness matrix
α, β, γ	weighting constants
ζ	vector of random variables
θ	vector of random parameters
θ_1, θ_2	vector of zero mean random parameters
λ_i	open-loop pole
μ_i	closed-loop pole
ρ	local weighting function
σ	objective function
Ψ_i	i^{th} multivariate Hermite polynomial

The receptance method, first formalised by Ram and Mottershead [5], is a methodology that performs pole placement, by means of active control, using measured receptances. The method is advantageous in that experimentally determined receptances are used directly and thus there is no need to know nor evaluate the mass, stiffness and damping matrices of the studied system. Whilst the method was originally developed for single-input systems, it has since been extended to the more general case of multiple-input-multiple-output systems [6] and has been implemented experimentally on a range of different systems. Tehrani et al. [7] applied the receptance method to both a lightweight glass-fibre beam with two smart-material sensors and actuators, and to a heavy modular test structure using various arrangements of accelerometers and electromechanical shakers. Fichera et al. [8] used the receptance method to suppress unstable vibrations on an aeroelastic wind-tunnel model. Similar work has also been carried out by Singh et al. [9,10] and Mokrani et al. [11], who have used the receptance method on an aeroelastic wing with multiple control surfaces. Tehrani and Mottershead [12] implemented the method on an AgustaWestland W30 helicopter airframe, modifying both the frequency and damping of the first two modes. In recent works, the method has also been extended to nonlinear systems [13,14].

Tehrani et al. [15] first studied the effect of uncertainty on the receptance method by considering the sensitivity of the placed poles to noise in measured receptances. By computing the infinity-norm of each row of eigenvalue sensitivities, poles were placed optimally within elliptical regions such that the local sensitivities were minimised. Liang et al. [16] later extended this work to consider how uncertainty in physical parameters, such as contact stiffness and contact damping, affected the spread of poles. By computing eigenvalue sensitivities through local perturbations, sensitivity matrices were constructed and their respective Frobenius norms were evaluated. Using a genetic algorithm, the closed-loop poles were iteratively placed so that the computed norms were minimised. Bai et al. [17], building upon their earlier work [18,19], introduced a robust quadratic eigenvalue assignment technique for systems with time delays, using measured receptances. Again, using an optimisation approach, poles were placed such that pole sensitivities were minimised according to the Frobenius norm. In [17], however, the objective function also included the norm of the control gains so that minimal control effort was required to shift the closed-loop poles. In all of the above-mentioned works, only local sensitivities have been considered.

In this research, a new globally optimum pole placement method that uses the method of receptances is presented. Using the Differential Evolution genetic optimisation algorithm by Storn and Price [20], closed-loop poles are iteratively placed within predefined rectangular regions such that the variance of the real and imaginary part of each pole is minimised. By using variances, the effect of the uncertainty is considered across its full range; it is not constrained only to its local effect at a nominal point. Variances are calculated using an efficient polynomial chaos (PC) expansion [21], which significantly reduces the number of samples required compared to other methods such as Monte Carlo simulation. Uncertainties in structural parameters are modelled as direct modifications to measured receptances so that no underlying model of the uncertain system is required. The method is demonstrated both numerically and experimentally on a multi-degree-of-freedom system.

The remainder of this paper is divided as follows; in Section 2, the theory is presented in the context of a single-input, linear, time-invariant (LTI) system. The method is then demonstrated numerically on a multi-degree-of-freedom system and is presented in a tutorial style in Section 3. Next, an experimental implementation of the method is considered in Section 4, which highlights its performance and applicability. Finally, the method is summarised and conclusions are drawn.

2. Theory

In this section, the theoretical basis of the method is described. First, a brief overview of the receptance method is provided. For simplicity, the method is shown using a single-input controller. Next, the process of modelling structural uncertainties is described together with an explanation of their effect on the system's poles. A method for uncertainty quantification of the poles is then given and is later used in a global optimisation approach to enable modification of the pole clusters in terms of size and shape. Finally, a summary of the method is illustrated diagrammatically.

2.1. The receptance method

Consider a linear dynamic system with dynamic stiffness matrix $\mathbf{Z} \in \mathbb{C}^{n\times n}$. When a full state feedback controller is used, the system is governed by

$$\mathbf{Z}(s)\mathbf{x}(s) = \mathbf{b}(s\mathbf{f}^T + \mathbf{g}^T)\mathbf{x}(s), \tag{1}$$

where $\mathbf{b} \in \mathbb{R}^n$ is the force distribution vector and $\mathbf{f}, \mathbf{g} \in \mathbb{R}^n$ are vectors of control gains. Pre-multiplying (1) by the receptance matrix,

$$\mathbf{H}(s) = \mathbf{Z}^{-1}(s), \tag{2}$$

gives

$$\mathbf{x}(s) = \mathbf{H}(s)\mathbf{b}(s\mathbf{f}^T + \mathbf{g}^T)\mathbf{x}(s). \tag{3}$$

When

$$\mathbf{r}_s = \mathbf{H}(s)\mathbf{b}, \tag{4}$$

(3) becomes

$$\mathbf{x}(s) = \mathbf{r}_s(s\mathbf{f}^T + \mathbf{g}^T)\mathbf{x}(s). \tag{5}$$

Suppose it is desired to shift the open-loop poles of the system $\{\lambda_1, \lambda_2, \ldots, \lambda_{2n}\}$ to a new set of desired closed-loop poles $\{\mu_1, \mu_2, \ldots, \mu_{2n}\}$. Substituting each closed-loop pole into (5) leads to

$$\mathbf{w}_k = \mathbf{r}_{\mu_k}(\mu_k\mathbf{f}^T + \mathbf{g}^T)\mathbf{w}_k, \quad k = 1, 2, \ldots, 2n, \tag{6}$$

where $\mathbf{w}_k$ is the eigenvector belonging to the k^{th} closed-loop pole. The non-trivial solution to (6) is

$$\mathbf{r}_{\mu_k}^T(\mu_k\mathbf{f} + \mathbf{g}) = 1, \quad \forall k, \tag{7}$$

which can be solved simultaneously to find $\mathbf{f}$ and $\mathbf{g}$. It should be noted that in order to obtain strictly real control gains, it is necessary that the set of closed-loop poles are closed under conjugation.

The above method has demonstrated how pole placement is performed using only receptances, which can be found experimentally. It is not necessary to construct the mass, stiffness and damping matrices of the system and therefore no model-form error is introduced.

2.2. Uncertainty modelling

Now, the effect of uncertainty in the structural parameters of the system is considered. Consider again the system represented by (1). When there exists uncertainty in p structural parameters, the dynamic stiffness matrix becomes a random matrix containing p independent random variables. Mathematically, the system is now written as

$$\mathbf{Z}(s, \boldsymbol{\theta})\mathbf{x}(s) = \mathbf{b}(s\mathbf{f}^T + \mathbf{g}^T)\mathbf{x}(s), \tag{8}$$

where $\boldsymbol{\theta} \in \mathbb{R}^p$ is the vector of random variables. By decomposing the dynamic stiffness matrix as the sum of a mean and random component,

$$\mathbf{Z}(s, \boldsymbol{\theta}) = \bar{\mathbf{Z}}(s) + \tilde{\mathbf{Z}}(s, \boldsymbol{\theta}_1), \tag{9}$$

where $\bar{\mathbf{Z}}$ and $\tilde{\mathbf{Z}}$ denotes the mean and random components of $\mathbf{Z}$ respectively, and $\boldsymbol{\theta}_1$ is given by

$$\boldsymbol{\theta}_1 = \boldsymbol{\theta} - \mathrm{E}[\boldsymbol{\theta}], \tag{10}$$

where E[•] is the expectation operator. The mean dynamic stiffness thus obeys

$$\bar{\mathbf{Z}}(s) = \mathrm{E}[\mathbf{Z}(s,\boldsymbol{\theta})]. \tag{11}$$

In practice, it is difficult to obtain an accurate estimate of the mean dynamic stiffness matrix experimentally. Indeed, due to the presence of the random parameters, any measured system is simply one outcome of the random system.

Let the dynamic stiffness matrix of a measured system be denoted $\mathbf{Z}_m(s)$. When the outcomes of the random variables cannot be measured, and so are unknown, the mean component in (9) is uncertain. Since the difference between the measured and mean system is caused by the random contribution, the mean dynamic stiffness matrix is now written as

$$\bar{\mathbf{Z}}(s,\boldsymbol{\theta}_2) = \mathbf{Z}_m(s) - \tilde{\mathbf{Z}}(s,\boldsymbol{\theta}_2), \tag{12}$$

where $\boldsymbol{\theta}_2$ has the same distribution as $\boldsymbol{\theta}_1$, but is independent. Replacing the mean dynamic stiffness in (9) with (12) gives that

$$\mathbf{Z}(s,\boldsymbol{\theta}) = \mathbf{Z}_m(s) + \tilde{\mathbf{Z}}(s,\boldsymbol{\theta}_1) - \tilde{\mathbf{Z}}(s,\boldsymbol{\theta}_2), \tag{13}$$

which may be simplified to

$$\mathbf{Z}(s,\boldsymbol{\theta}) = \mathbf{Z}_m(s) + \tilde{\mathbf{Z}}(s,\boldsymbol{\theta}_t), \tag{14}$$

where

$$\boldsymbol{\theta}_t = \boldsymbol{\theta}_1 - \boldsymbol{\theta}_2. \tag{15}$$

In this form, the effect of the random parameters on the dynamic stiffness matrix is taken as a single perturbation about a randomly selected nominal, random system; there is no assumption about the mean dynamic stiffness. The single perturbation is comprised of two elements: $\boldsymbol{\theta}_1$, which represents the uncertainty due to the randomness in the manufacturing process itself; and $\boldsymbol{\theta}_2$, which represents the uncertainty that arises from being unable to measure the outcome of the random parameters in the measured system.

Substituting (14) into (8) and re-arranging leads to

$$\left(\mathbf{Z}_m(s) + \tilde{\mathbf{Z}}(s,\boldsymbol{\theta}_t) - \mathbf{b}(s\mathbf{f}^T + \mathbf{g}^T)\right)\mathbf{x}(s) = \mathbf{0}. \tag{16}$$

Pre-multiplying by the measured receptance matrix $\mathbf{H}_m(s)$ results in

$$\left(\mathbf{I} + \mathbf{H}_m(s)\tilde{\mathbf{Z}}(s,\boldsymbol{\theta}_t) - \mathbf{H}_m(s)\mathbf{b}(s\mathbf{f}^T + \mathbf{g}^T)\right)\mathbf{x}(s) = \mathbf{0}, \tag{17}$$

and thus the closed-loop, random poles are given by

$$\det\left[\mathbf{I} + \mathbf{H}_m(s)\tilde{\mathbf{Z}}(s,\boldsymbol{\theta}_t) - \mathbf{H}_m(s)\mathbf{b}(s\mathbf{f}^T + \mathbf{g}^T)\right] = 0 \tag{18}$$

The effect of the controller and the random contribution in (18) can be considered successively. First, the term $\mathbf{H}_m(s)\mathbf{b}(s\mathbf{f}^T + \mathbf{g}^T)$ serves to shift the open-loop, nominal poles to a new set, which are denoted the 'closed-loop, nominal poles'. The term $\mathbf{H}_m(s)\tilde{\mathbf{Z}}(s,\boldsymbol{\theta}_t)$ then shifts the closed-loop, nominal poles randomly to a new set of 'closed-loop, random poles'. The resulting spread of closed-loop poles are referred to as 'pole clusters' hereinafter. Since

$$\mathrm{E}\left[\tilde{\mathbf{Z}}(s,\boldsymbol{\theta}_t)\right] = \mathbf{0}_{n\times n}, \tag{19}$$

the pole clusters are spread about the closed-loop, nominal poles. This effect can be seen in Section 3.

The size and shape of the pole clusters is shown to be dependent on the location of the closed-loop, nominal poles. That is to say that the control gains not only affect the position of the nominal poles, but also the extent to which the uncertainty modifies the poles clusters. It is hypothesized, therefore, that there exists some optimum set of control gains such that the size and shape of the pole clusters are optimised. In order to determine the optimum gains, it is necessary to numerically quantify the geometry of the pole clusters.

2.3. Uncertainty quantification & optimisation of the poles

In previous works, pole cluster variability has been quantified using local sensitivities. In this paper, however, global variability is considered by using the variance of the real and imaginary parts of each pole cluster. In this way, the uncertainty in the pole clusters is considered across the full range of the random structural parameters. The simplest way to obtain the pole cluster variances is to use Monte Carlo simulation. However, this is computationally expensive and requires a large number of samples in order to achieve sufficiently accurate estimates. Instead, polynomial chaos (PC) expansions can be used, which significantly reduces the number of samples needed.

PC expansions use a series of orthogonal functions to form a surrogate model of a random function of one or more independent random variables. When the independent variables follow a standard normal distribution, the PC expansion may be written as

$$y(\zeta) = \sum_{i=0}^{\infty} a_i \Psi_i(\zeta), \tag{20}$$

where $y : \mathbb{R} \to \mathbb{R}$ is the random function, $a_i \in \mathbb{R}$ are constants of the expansion, $\zeta \in \mathbb{R}^p$ is the vector of independent random variables, and Ψ_i is the i^{th} multivariate Hermite polynomial. For computational implementation, the expansion is truncated to the first N terms and therefore

$$y(\zeta) \approx \sum_{i=0}^{N-1} a_i \Psi_i(\zeta). \tag{21}$$

One way to determine the coefficients of the expansion is to perform sampling across a set of random functions and independent variables. With relatively few samples, a linear regression can be used to fit the expansion through the sampled data [22].

Once the constants of the expansion are determined, the variance of the dependent variable may be approximated as [23]

$$\mathrm{Var}[y(\zeta)] \approx \sum_{i=1}^{N-1} a_i^2 \mathrm{E}\left[\Psi_i^2(\zeta)\right]. \tag{22}$$

In this particular work, the random functions are the real and imaginary parts of each pole and the independent variables are the random structural parameters. Thus for an n degree-of-freedom system, there are $4n$ expansion; one for the real and imaginary part of each pole.

With expressions for the variances found, an optimisation approach can now be used so that they are reduced according to some defined objective function. For each random pole, a local weighting function is defined as

$$\rho_i = \alpha_i \mathrm{Var}\left[\mathrm{Re}(\mu_i)\right] + \beta_i \mathrm{Var}\left[\mathrm{Im}(\mu_i)\right], \quad i = 1, 2, \ldots 2n, \tag{23}$$

where $\alpha_i, \beta_i \in \mathbb{R}$ are constants that weight the relative importance of the variance of the real and imaginary part of each random pole. Then, by defining the objective function as

$$\sigma = \sum_{i=1}^{2n} \gamma_i \rho_i, \tag{24}$$

where $\gamma_i \in \mathbb{R}$ are additional weighting constants, it is now possible to weight the relative importance of each pole. In theory, selection of appropriate weighting constants in (23) and (24) permits the alteration of the size and shape of pole clusters, as will be demonstrated in the numerical examples later.

In practice, the maximum control authority governs the extent to which the poles can be modified. Moreover, large deviations from the initial set of open-loop, nominal poles may lead to non-physical natural frequencies and damping. As a result, nominal, closed-loop pole constraints are used.

For each nominal pole, the constraints

$$\mathrm{Re}_{\min}(\mu_i) \leqslant \mathrm{Re}(\mu_i) \leqslant \mathrm{Re}_{\max}(\mu_i), \quad i = 1, 2, \ldots, 2n, \tag{25}$$

and

$$\mathrm{Im}_{\min}(\mu_i) \leqslant \mathrm{Im}(\mu_i) \leqslant \mathrm{Im}_{\max}(\mu_i), \quad i = 1, 2, \ldots, 2n, \tag{26}$$

are introduced. These constraints force the closed-loop, nominal poles to be within rectangular boxes in the complex plane.

2.4. Method overview

An overview of the method is illustrated in Fig. 1.

3. Numerical examples

3.1. Example 1: One random parameter

Consider a three-degree-of-freedom system with mass, damping and stiffness matrices

$$\mathbf{M} = \begin{bmatrix} 1.5 & 0 & 0 \\ 0 & m_2 & 0 \\ 0 & 0 & 1.2 \end{bmatrix}, \mathbf{C} = \begin{bmatrix} 4 & -1 & 0 \\ -1 & 5 & -1 \\ 0 & -1 & 4 \end{bmatrix}, \mathbf{K} = \begin{bmatrix} 3000 & -1000 & 0 \\ -1000 & 3000 & -1000 \\ 0 & -1000 & 3000 \end{bmatrix},$$

where

$$m_2 \sim \mathcal{N}(2.0, 0.01),$$

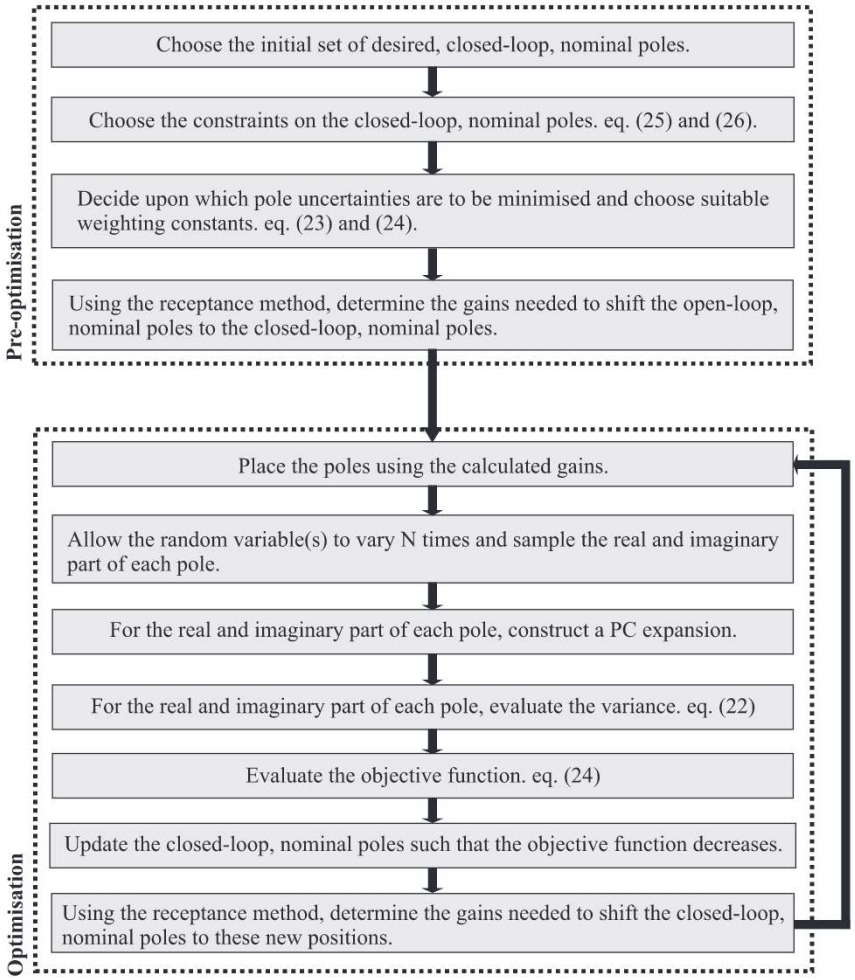

Fig. 1. Method overview.

and force distribution vector

$$\mathbf{b} = [-1 \quad 0 \quad 0]^T.$$

Suppose that an outcome of the random system is measured[1] and has a receptance matrix

$$\mathbf{H} = \begin{bmatrix} 1.5s^2 + 4s + 3000 & -s - 1000 & 0 \\ -s - 1000 & 2.03s^2 + 5s + 3000 & -s - 1000 \\ 0 & -s - 1000 & 1.2s^2 + 4s + 3000 \end{bmatrix}^{-1}.$$

with corresponding open-loop poles

$$\begin{aligned} \lambda_{1,2} &= -0.9111 \pm 30.2487i, \\ \lambda_{3,4} &= -1.4475 \pm 46.5577i, \\ \lambda_{5,6} &= -1.8730 \pm 53.7473i. \end{aligned}$$

Writing the uncertainty in the mass m_2 as a perturbation about the nominal dynamic stiffness, as in (9),

$$\tilde{\mathbf{Z}}(s, \theta_1) = \begin{bmatrix} 0 & 0 & 0 \\ 0 & m_r s^2 & 0 \\ 0 & 0 & 0 \end{bmatrix},$$

[1] For the purposes of this numerical example, the outcome is taken as $m_2 = 2.03$ kg. Of course, in practice, the outcome cannot be measured and is thus unknown.

where

$$m_r \sim \mathcal{N}(0, 0.01).$$

As explained in Section 2.2, the particular outcome of m_2 in the measured system is unknown and thus the nominal dynamic stiffness is also unknown. Consequently, the uncertainty must be treated as a perturbation about the *measured* value. Using (13),

$$\tilde{\mathbf{Z}}(s, \theta_t) = \begin{bmatrix} 0 & 0 & 0 \\ 0 & m_{r,1}s^2 & 0 \\ 0 & 0 & 0 \end{bmatrix} - \begin{bmatrix} 0 & 0 & 0 \\ 0 & m_{r,2}s^2 & 0 \\ 0 & 0 & 0 \end{bmatrix} = \begin{bmatrix} 0 & 0 & 0 \\ 0 & (m_{r,1} - m_{r,2})s^2 & 0 \\ 0 & 0 & 0 \end{bmatrix}, \tag{27}$$

where $m_{r,1}$ and $m_{r,2}$ are independent random variables with the same distribution of m_r. Since $m_{r,1}$ and $m_{r,2}$ are normally distributed, (27) may be simplified to

$$\tilde{\mathbf{Z}}(s, \theta_t) = \begin{bmatrix} 0 & 0 & 0 \\ 0 & m_{r,t}s^2 & 0 \\ 0 & 0 & 0 \end{bmatrix},$$

where

$$m_{r,t} \sim \mathcal{N}(0, 0.02).$$

Suppose that the open-loop poles are to be shifted to a new set with constraints as given in Table 1. If it is desired that the variance of the real part of the third pole pair is to be minimised, the objective function is chosen as

$$\sigma = \mathrm{Var}\left[\mathrm{Re}(\mu_6)\right]. \tag{28}$$

Performing the optimisation using 3^{rd} order PC expansions constructed by 50 samples and using the open-loop poles as the initial set, the optimum set is found to be

$$\begin{aligned} \mu_{1,2} &= -2.0191 \pm 33.2487i, \\ \mu_{3,4} &= -1.5805 \pm 45.9539i, \\ \mu_{5,6} &= -2.0730 \pm 54.7204i, \end{aligned}$$

which is achieved using control gains

$$\mathbf{f} = [4.3232 \quad 6.6404 \quad 2.9018]^T, \quad \mathbf{g} = [368.1 \quad 387.5 \quad 596.4]^T.$$

The objective function is reduced from 1.3×10^{-3} to 3.6×10^{-8}. Fig. 2 illustrates the pole variability before and after the receptance control gains are applied. As desired, the geometry of the pole cluster associated with the third mode is now modified in such a way that it varies less in the real axis direction. This is, however, at the expense of a larger variability in the first and second mode.

To ensure that the real part variation of the first and second mode is not increased beyond acceptable levels, the objective function can be changed to

$$\sigma = 100 \times \mathrm{Var}\left[\mathrm{Re}(\mu_5)\right] + \mathrm{Var}\left[\mathrm{Re}(\mu_1)\right] + \mathrm{Var}\left[\mathrm{Re}(\mu_3)\right]. \tag{29}$$

Now, the objective function also includes both the variances of the real part of the first and second pole pairs. In this way, a large variability in these poles penalises the objective function. The variance of the third pole is weighted higher than the other poles. This is so that the variability of the third pole has a greater penalty than the others and thus the optimisation searches in such a way that considers the variability of the third pole pair to be of greater importance. Re-running the optimisation, with the same settings as before, the new optimum set of closed-loop poles is computed as

$$\begin{aligned} \mu_{1,2} &= -1.9111 \pm 27.2487i, \\ \mu_{3,4} &= -1.2475 \pm 43.5577i, \\ \mu_{5,6} &= -1.6729 \pm 50.7473i, \end{aligned}$$

which is achieved using control gains of

Table 1
Closed-loop pole constraints (numerical - example 1).

Pole	$\mathrm{Re}(\mu)_{\min}$	$\mathrm{Re}(\mu)_{\max}$	$\lvert\mathrm{Im}(\mu)\rvert_{\min}$	$\lvert\mathrm{Im}(\mu)\rvert_{\max}$
$\mu_{1,2}$	−2.3111	−1.9111	27.2487	33.2487
$\mu_{3,4}$	−1.6475	−1.2475	43.5577	49.5577
$\mu_{5,6}$	−2.0730	−1.6730	50.7473	56.7473

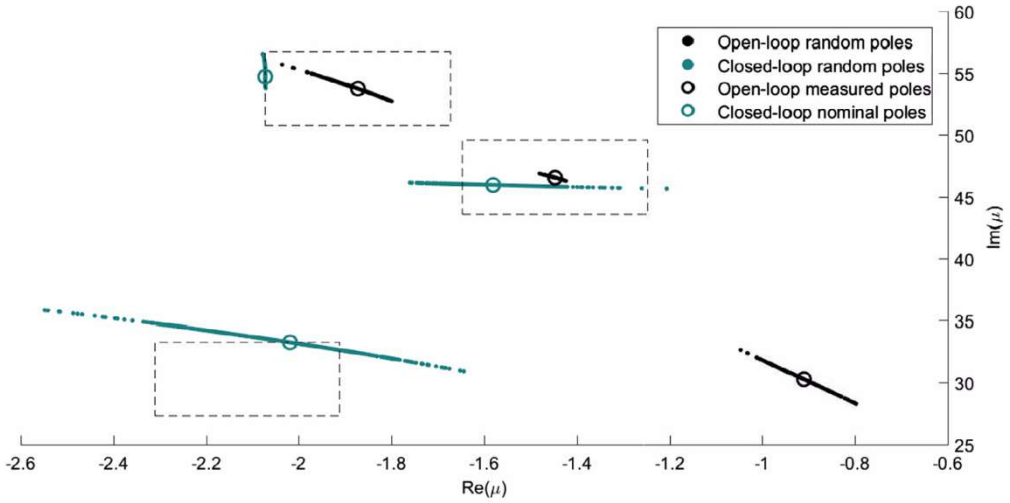

Fig. 2. Open- and closed-loop pole variability (objective function 1).

$$\mathbf{f} = [1.8002 \quad 5.2514 \quad 0.5826]^T, \quad \mathbf{g} = [-1134 \quad 999.4 \quad -1583]^T.$$

The objective function now decreases from 1.4×10^{-1} to 5.0×10^{-3}. Fig. 3 shows the variability of the new closed-loop poles. As before, the real part variation of the first mode is reduced. Although the reduction is not as significant, the variability of the first and second mode is now not as large.

At this point, the need to use global measures to quantify pole uncertainties becomes clear. Consider again the pole cluster belonging to the second mode in Fig. 3. Given its large curvature, local sensitivities, which quantify uncertainty using only first order information, would not capture the variability well. Indeed, it would only quantify uncertainty in the region near to the nominal pole and thus neglect the full range of the random parameters. By contrast, variances do not rely on low-order approximations and so quantify the uncertainty globally.

3.2. Example 2: multiple random parameters

Consider again the system in Example 1, but now with modified mass matrix

$$\mathbf{M} = \begin{bmatrix} m_1 & 0 & 0 \\ 0 & m_2 & 0 \\ 0 & 0 & m_3 \end{bmatrix},$$

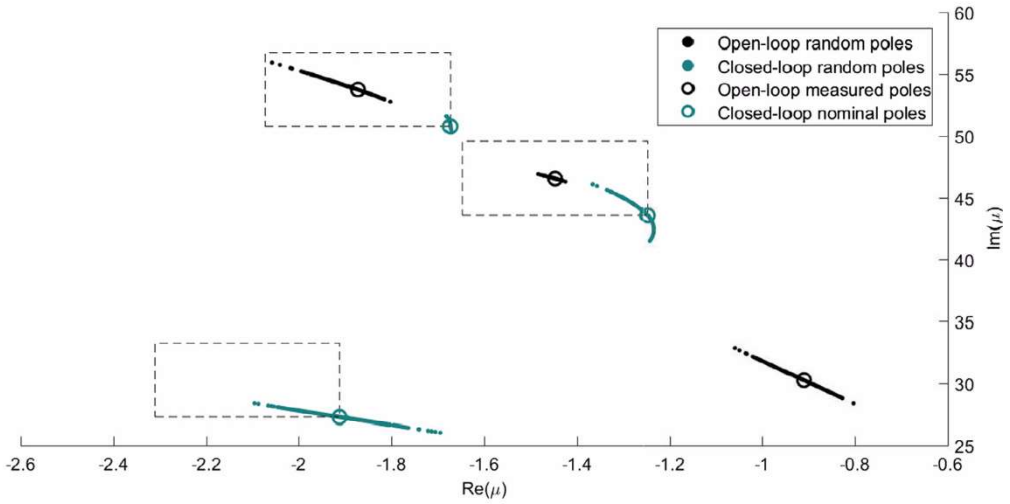

Fig. 3. Open- and closed-loop pole variability (objective function 2).

where

$$m_1 \sim \mathcal{N}(1.5, 0.01), m_2 \sim \mathcal{N}(2.0, 0.01), m_3 \sim \mathcal{N}(1.2, 0.01),$$

In this case, all three masses are uncertain and thus there are now three random parameters.

Suppose that an outcome of the new random system is measured and has a receptance matrix of

$$\mathbf{H} = \begin{bmatrix} 1.6s^2 + 4s + 3000 & -s - 1000 & 0 \\ -s - 1000 & 2.03s^2 + 5s + 3000 & -s - 1000 \\ 0 & -s - 1000 & 1.12s^2 + 4s + 3000 \end{bmatrix}^{-1}.$$

and corresponding open-loop poles of

$$\begin{aligned} \lambda_{1,2} &= -0.8998 \pm 30.1019i, \\ \lambda_{3,4} &= -1.3953 \pm 45.6534i, \\ \lambda_{5,6} &= -1.9105 \pm 54.2425i. \end{aligned}$$

Now writing the uncertainty in the three masses as a perturbation about the *measured* system, as in (13), and simplifying as before

$$\tilde{\mathbf{Z}}(s, \theta_t) = \begin{bmatrix} m_{1,t}s^2 & 0 & 0 \\ 0 & m_{2,t}s^2 & 0 \\ 0 & 0 & m_{3,t}s^2 \end{bmatrix}, \tag{30}$$

where $m_{1,t}, m_{2,t}$ and $m_{3,t}$ are independent random variables with distribution

$$m_1, m_2, m_3 \sim \mathcal{N}(0, 0.02).$$

Suppose now that the open-loop poles are to be shifted to a new set with constraints as given in Table 2. Note that the constraints enforce the restriction that no poles may move further right in the complex plane. If it is desired that the variance of the imaginary and real part of the second conjugate pair of poles is to be minimised, the objective function is chosen as

$$\sigma = \mathrm{Var}[\mathrm{Im}(\mu_3)] + 1000 \times \mathrm{Var}[\mathrm{Re}(\mu_3)]. \tag{31}$$

Note that the weighting constants here serve to scale the variance of the real and imaginary parts to a comparable level. Performing the optimisation using 3*rd* order PC expansions constructed by 1000 samples and using the open-loop poles as the initial set, the optimum set is found to be

$$\begin{aligned} \mu_{1,2} &= -1.8998 \pm 27.1019i, \\ \mu_{3,4} &= -1.3953 \pm 48.6534i, \\ \mu_{5,6} &= -2.0885 \pm 53.6353i, \end{aligned}$$

which is achieved using control gains of

$$\mathbf{f} = [3.7694 \quad 6.9049 \quad 3.7324]^T, \quad \mathbf{g} = [78.13 \quad -676.7 \quad -612.6]^T.$$

Fig. 4 illustrates the pole variability before and after the receptance control gains are applied. In this case, the objective function increases from 10.5 in the open-loop to 18.3 in the closed-loop. This means that, regardless of where the poles are placed in the constraint boxes, the variability of the mode of interest will always become worse. As a consequence, the result obtained from the optimisation can only give the best solution for the chosen constraint boxes.

4. Experimental implementation

In this section, an experimental implementation of the method is described. First, the set-up is outlined and the open-loop frequency response functions (FRFs) and poles are given. Two experiments, each with their own optimisation goal, are then presented together with a brief physical interpretation of the optimisation's result. For the purposes of simplicity, both experiments will consider only one uncertain parameter.

Table 2
Closed-loop pole constraints (numerical - example 2).

Pole	$\mathrm{Re}(\mu)_{\min}$	$\mathrm{Re}(\mu)_{\max}$	$\lvert\mathrm{Im}(\mu)\rvert_{\min}$	$\lvert\mathrm{Im}(\mu)\rvert_{\max}$
$\mu_{1,2}$	−2.2998	−1.8998	27.1019	33.1019
$\mu_{3,4}$	−1.7953	−1.3953	42.6534	48.6534
$\mu_{5,6}$	−2.3105	−1.9105	51.2425	57.2425

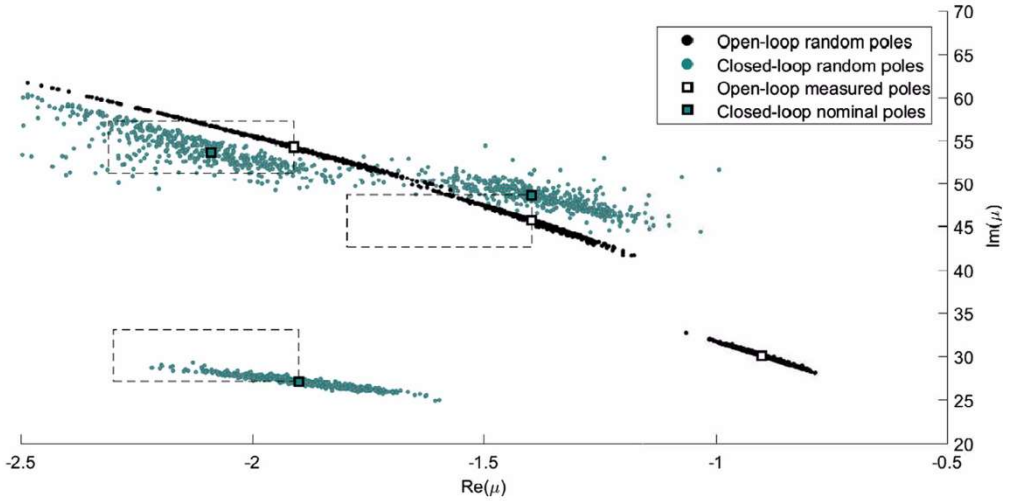

Fig. 4. Open- and closed-loop pole variability (objective function 3).

4.1. Set-up

Experiments were conducted on a three-degree-of-freedom mass-spring system, which is shown in Fig. 5. The system consisted of three block masses connected by a series of thin steel plates that served as spring elements. The mass of the middle block, which was considered uncertain, was varied by adding or removing up to six 0.1 kg masses. Throughout the tests, the nominal, measured system was defined as the original structure plus three small masses (0.3 kg). This allowed the effect of adding and removing masses to be considered equally. The leftmost mass was actuated by an electromechanical shaker. It was through this shaker that the control force was applied and thus the corresponding force distribution vector was

$$\mathbf{b} = [-1 \quad 0 \quad 0]^T.$$

The force input to the system was measured by a load cell and the positions of the masses were measured using three laser displacement sensors (LDS).

Since force feedback is used in these experiments, a PID was required to output a desired force, as measured by the load cell, from a voltage input to the amplifier. The Ziegler-Nichols method [24] was used initially to tune the PID gains before they were manually adjusted to optimise performance. The final transfer function of the PID was

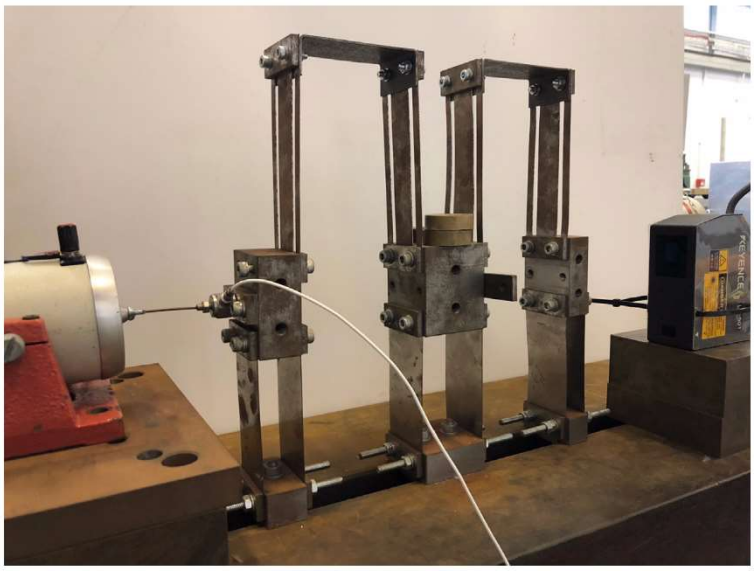

Fig. 5. Experimental mass-spring system.

$$\frac{F(s)}{E(s)} = \frac{0.002s^2 + 1.4s + 400}{s},$$

and remained constant throughout both experiments. The PID and high-level feedback control were both implemented in a real-time processing environment. This arrangement is illustrated diagrammatically in Fig. 6. As shown, 2*nd* order Butterworth filters with a cut-off frequency of 40 Hz were used on both the force and LDS outputs. This was necessary because the signals were differentiated and therefore it was essential remove unwanted noise and disturbances.

The open-loop receptances of the system were collected by means of impact hammer testing. With the PID active, but setting all of the receptance control gains to zero, the desired controller input to the system was held at 0 N. An impact was then imparted on each mass and FRFs at each sensor measured. The advantage of collecting FRFs of the open-loop system in this way is that the dynamics of the PID, shaker and filters were all included and thus the only change in the closed-loop testing was the receptance gains. Fig. 7 shows the open-loop measured FRFs and the curve fits using a normal modes assumption [25].

The open-loop, nominal poles were found to be

$$\begin{aligned} \lambda_{1,2} &= -0.3530 \pm 41.39i, \\ \lambda_{3,4} &= -0.9760 \pm 57.71i, \\ \lambda_{5,6} &= -0.1475 \pm 72.12i, \end{aligned}$$

In order to visualise the effect of the uncertainty, 0.3 kg was added to and removed from the middle mass in increments of 0.1 kg. Fig. 8 shows the FRF variability at H_{11}. As shown, the frequency of the first, second and third mode vary by 0.7028 Hz, 0.1707 Hz and 0.1440 Hz respectively.

In the proceeding experiments, the variability of the first two modes are to be minimised using pole placement according to the constraints given in Table 3. Given the low damping of the third mode in the open-loop testing, it was decided that the limits on the real parts would be strongly constrained to greater negative values than in the open-loop in order to prevent the system becoming unstable.

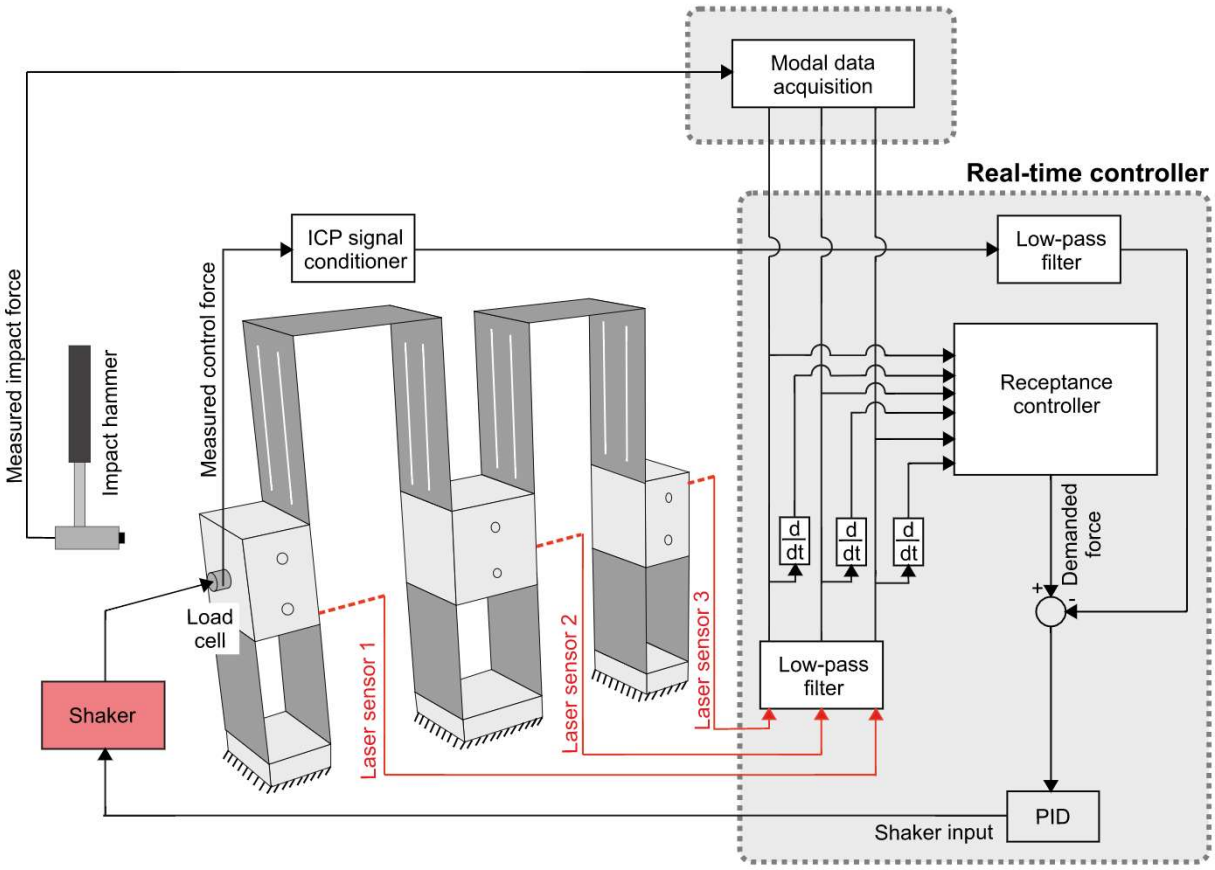

Fig. 6. System interconnection diagram.

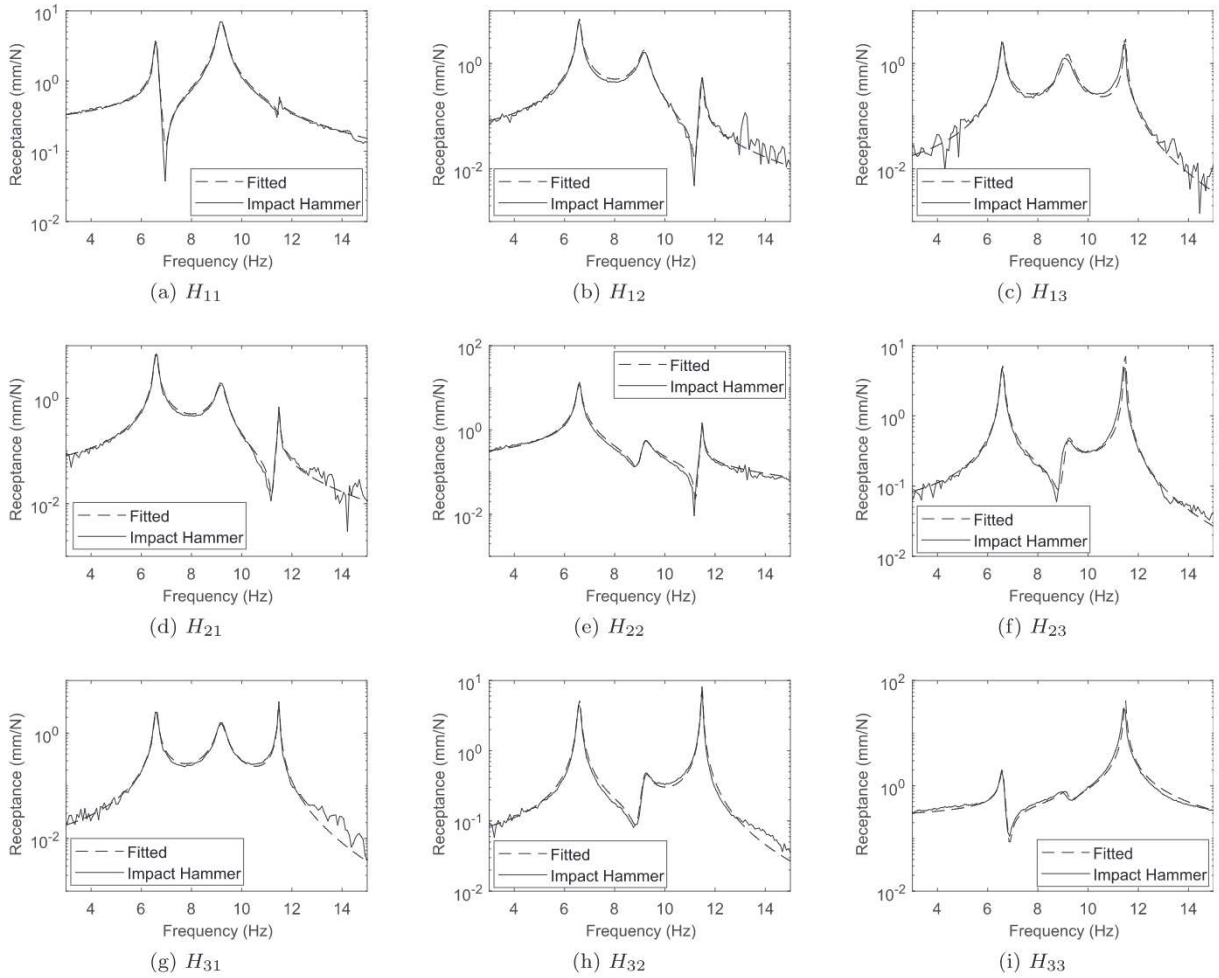

Fig. 7. Measured and fitted open-loop FRFs.

4.2. Experiment 1: frequency variability of the second mode

In the first experiment, it was desired to minimise the imaginary part variation of the second mode. This is equivalent to minimising the variation of the frequency of this mode. Selecting

$$\sigma = \mathrm{Var}[\mathrm{Im}(\mu_3)]$$

as the objective function, the optimisation was performed using 3*rd* order PC expansions constructed by 50 samples from a normal distribution with zero mean and a standard deviation of 0.14 kg. Note that the zero mean condition arises from (10) and the standard deviation is chosen such that ± 2 standard deviations are shown experimentally. The optimum closed-loop, nominal poles were found to be

$$\begin{aligned} \mu_{1,2} &= -0.544 \pm 43.87i, \\ \mu_{3,4} &= -0.928 \pm 59.20i, \\ \mu_{5,6} &= -0.537 \pm 72.00i, \end{aligned}$$

which required the control gains

$$\mathbf{f} = [1.2861 \quad -1.2736 \quad 7.4807]^T, \quad \mathbf{g} = [494.43 \quad 888.06 \quad -30.78]^T.$$

Numerically, the objective function decreased from 5.20×10^{-2} to 3.26×10^{-8}. This meant that the imaginary part of the pole was shifted to a location in the complex plane where it was close to being invariant. With the control gains applied, Fig. 9 shows the FRF of the closed-loop system as the middle mass was modified between ± 0.3 kg. It was found that the frequency of the second mode now varied by 0.0316 Hz, a reduction from the open-loop case of 81.49%.

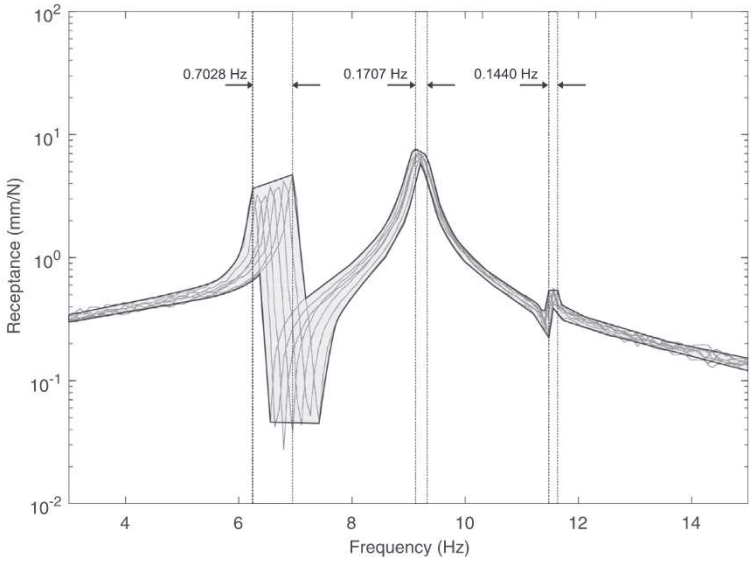

Fig. 8. Open-loop FRF variability at H_{11} between ±0.3 kg.

Table 3
Closed-loop pole constraints (experimental).

Pole	$\mathrm{Re}(\mu)_{\min}$	$\mathrm{Re}(\mu)_{\max}$	$\lvert\mathrm{Im}(\mu)\rvert_{\min}$	$\lvert\mathrm{Im}(\mu)\rvert_{\max}$
$\mu_{1,2}$	−0.55	−0.35	38.39	44
$\mu_{3,4}$	−1.07	−0.87	57.7	59.7
$\mu_{5,6}$	−0.60	−0.50	72.0	72.2

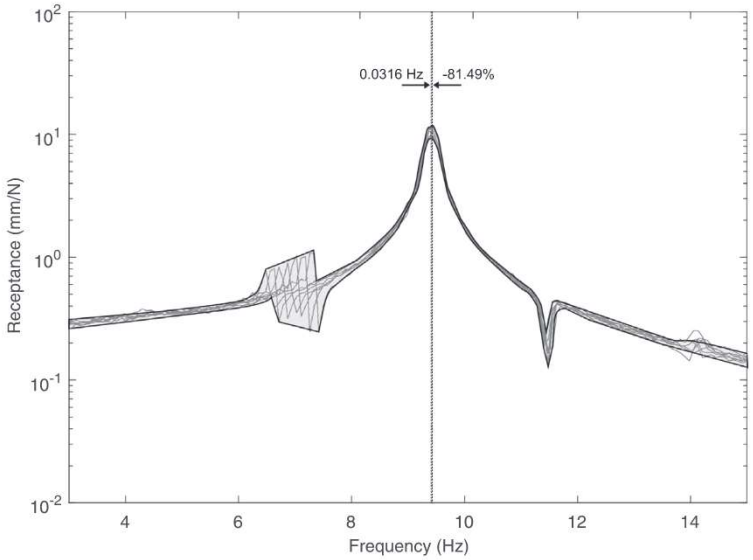

Fig. 9. Closed-loop FRF variability at H_{11} between ±0.3 kg - experiment 1.

Physical insight of the optimisation result may be found by examining the closed-loop, nominal FRF at H_{22}, as shown in Fig. 10. In comparison with its open-loop counterpart, the displacement of the second mass in the second mode is now smaller. Moreover, the zero to the left of the peak is now closer to the pole of the second mode. Therefore, it appears that the optimisation is attempting to assign a node such that the amplitude of the second mass in the second mode is much smaller.

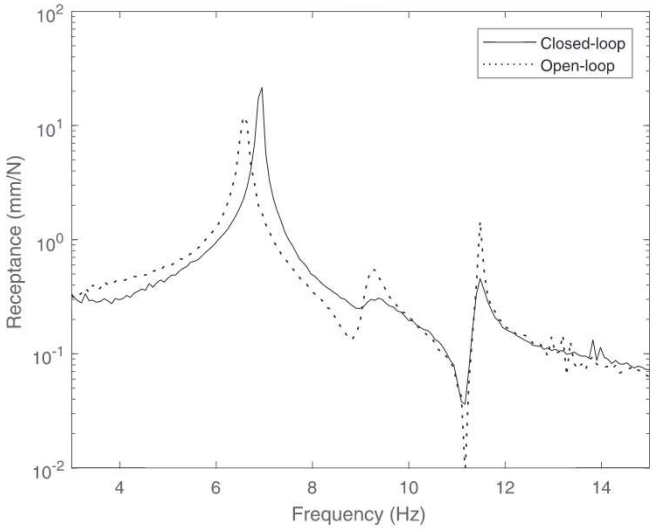

Fig. 10. Nominal closed-loop FRF at H_{22}.

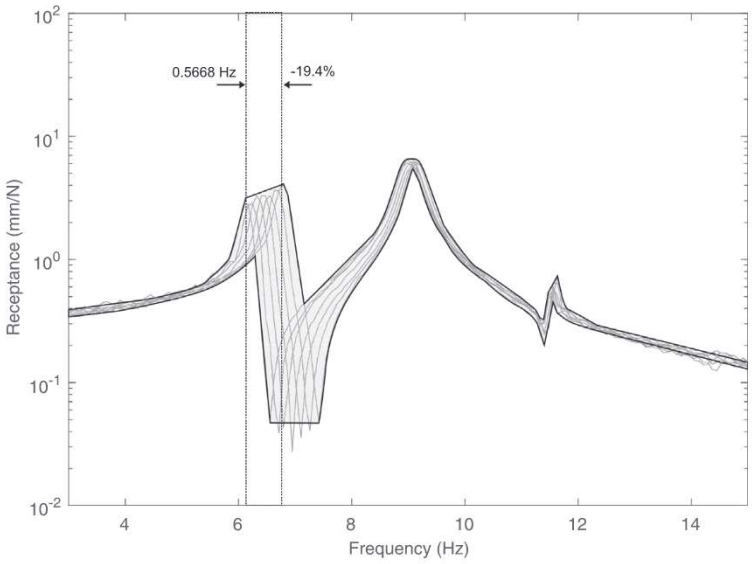

Fig. 11. Closed-loop FRF variability at H_{11} between ± 0.3 kg - experiment 2.

In this way, the effect of adding a mass to this position is very small and thus has little impact upon the frequency variation, as was desired.

4.3. Experiment 2: frequency variability of the first mode

In the second experiment, it was desired to minimise the frequency variation of the first mode. Using the same optimisation settings as the first experiment but selecting

$$\sigma = \mathrm{Var}\left[\mathrm{Im}(\mu_1)\right]$$

as the objective function, the optimum closed-loop nominal poles were found to be

$$\begin{aligned} \mu_{1,2} &= -0.400 \pm 38.39i, \\ \mu_{3,4} &= -0.870 \pm 57.70i, \\ \mu_{5,6} &= -0.594 \pm 72.00i, \end{aligned}$$

which required control gains of

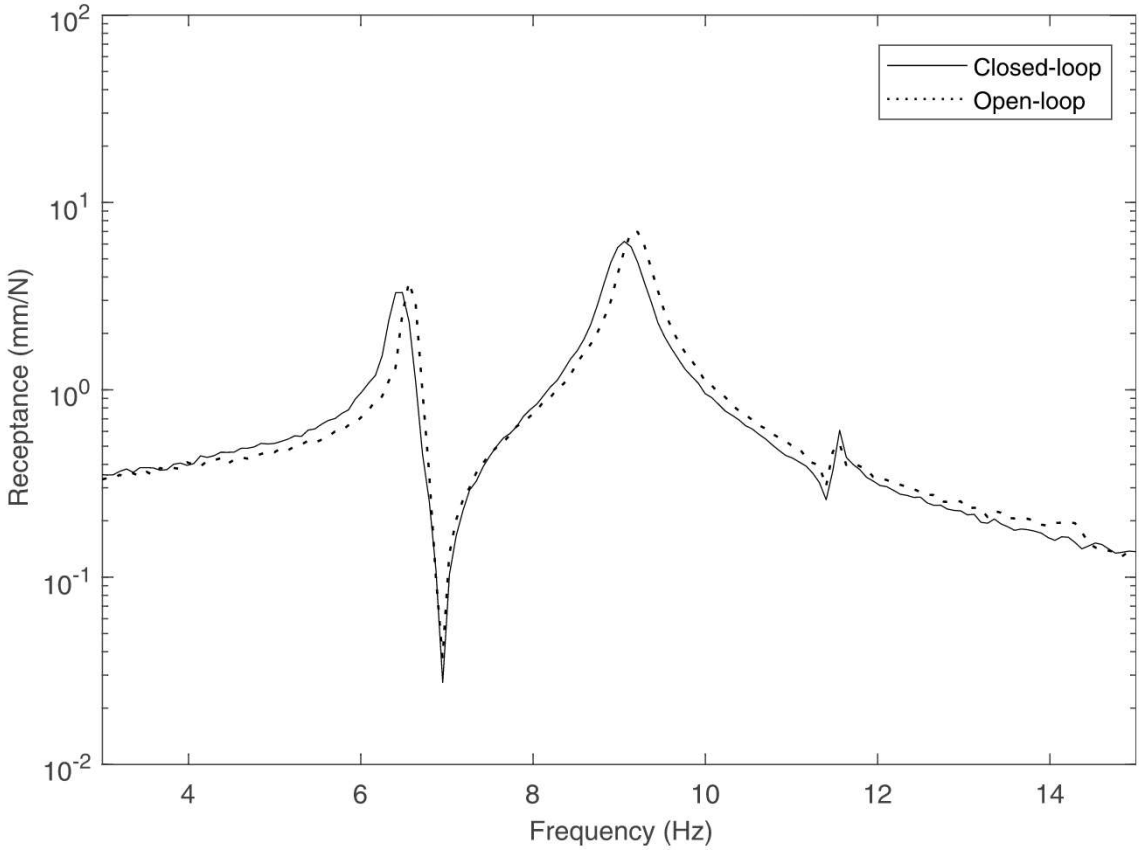

Fig. 12. Nominal closed-loop FRF at H_{11}.

$$\mathbf{f} = [0.8867 \quad -3.8621 \quad 9.9066]^T, \quad \mathbf{g} = [-306.38 \quad -863.89 \quad -388.20]^T.$$

Numerically, the objective function decreased from 1.3920 to 0.8904, a change of −36%. Experimentally, the frequency variation in the first mode become 0.5668 Hz, a reduction of 19.4% from the open-loop, as shown in Fig. 11.

Notably, the reduction of the frequency variation in this second experiment is not as large as the first experiment. This is likely due to the fact that assignment of a node to the second mass in the first mode would require extremely large control gains; in other words, the closed-loop poles would have to be moved to locations well outside of the constraint boxes. This is confirmed in Fig. 12, which shows that the location of the zero, in terms of frequency, remains unchanged before and after the control gains are applied.

5. Conclusions

This paper has presented a new method for optimal pole placement in dynamic systems with uncertain structural parameters. It has been shown that, by coupling pole placement with a global optimisation algorithm based on the variance of the real and imaginary part of each pole, it is possible to modify the size and shape of pole clusters such that they satisfy some desired performance criterion. The method is advantageous in that: (i) uncertainty in structural parameters is evident in measured receptance data directly; (ii) there is no requirement to measure receptances for the mean system; (iii) by using variances calculated by a polynomial chaos expansion, the effect of the uncertainty is considered across its full range.

The method has been tested both numerically and experimentally. In both cases, it is shown that appropriate selection of objective functions allows significant reduction of the above-mentioned variances. Experimentally, it has been demonstrated that it can reduce the variation of the frequency of a mode by approximately 81% across the ranges tested.

Acknowledgement

The authors wish to acknowledge the support provided by the EPSRC Doctoral Training Scholarship and EPSRC grant EP/N017897/1.

References

[1] S. Daouk, F. Louf, O. Dorival, L. Champaney, S. Audebert, Uncertainties in structural dynamics: overview and comparative analysis of methods, Mech. Ind. 16 (4) (2015) 404.
[2] S.K. Choi, R.V. Grandhi, R.A. Canfield, Reliability-based Structural Design, 1st Edition., Springer, New York, 2007.
[3] A. Chateauneuf, Principles of reliability-based design optimization, in: Y. Tsompanakis, N.D. Lagaros, M. Papadrakakis (Eds.), Structural Design Optimization Considering Uncertainties, first ed., Taylor & Francis, London, 2008, pp. 3–30.
[4] J.E. Mottershead, Y.M. Ram, Inverse eigenvalue problems in vibration absorption: Passive modification and active control, Mech. Syst. Signal Process. 20 (1) (2006) 5–44.
[5] Y.M. Ram, J.E. Mottershead, Receptance method in active vibration control, AIAA J. 45 (3) (2007) 562–567.
[6] Y.M. Ram, J.E. Mottershead, Multiple-input active vibration control by partial pole placement using the method of receptances, Mech. Syst. Signal Process. 40 (2) (2013) 727–735.
[7] M.G. Tehrani, R.N. Elliott, J.E. Mottershead, Partial pole placement in structures by the method of receptances: theory and experiments, J. Sound Vib. 329 (24) (2010) 5017–5035.
[8] S. Fichera, S. Jiffri, J.E. Mottershead, Design and wind tunnel test of a MODular aeroelastic FLEXible wing (MODFLEX), in: Proceedings of the International Conference on Noise and Vibration Engineering ISMA 2016, 2016, pp. 445–456.
[9] K.V. Singh, L.A. McDonough, R. Kolonay, J.E. Cooper, Receptance-based active aeroelastic control using multiple control surfaces, J. Aircraft 51 (1) (2014) 335–342.
[10] K.V. Singh, R.N. Brown, R. Kolonay, Receptance-based active aeroelastic control with embedded control surfaces having actuator dynamics, J. Aircraft 53 (3) (2016) 830–845.
[11] B. Mokrani, F. Palazzo, S. Fichera, L.J. Adamson, J.E. Mottershead, Multi-input multi-output aeroelastic control using the receptance method, in: Proceedings of the International Conference on Noise and Vibration Engineering ISMA 2018, 2018, pp. 153–163.
[12] M.G. Tehrani, J. Mottershead, An overview of the receptance method in active vibration control, IFAC Proceedings Volumes, vol. 45, IFAC, 2012, pp. 1174–1178.
[13] M.G. Tehrani, L. Wilmshurst, S.J. Elliott, Receptance method for active vibration control of a nonlinear system, J. Sound Vib. 332 (19) (2013) 4440–4449.
[14] C. Zhen, S. Jiffri, D. Li, J. Xiang, J.E. Mottershead, Feedback linearisation of nonlinear vibration problems: a new formulation by the method of receptances, Mech. Syst. Signal Process. 98 (2018) 1056–1068.
[15] M.G. Tehrani, J.E. Mottershead, A.T. Shenton, Y.M. Ram, Robust pole placement in structures by the method of receptances, Mech. Syst. Signal Process. 25 (1) (2011) 112–122.
[16] Y. Liang, H. Yamaura, H. Ouyang, Active assignment of eigenvalues and eigen-sensitivities for robust stabilization of friction-induced vibration, Mech. Syst. Signal Process. 90 (2017) 254–267.
[17] Z.J. Bai, J.K. Yang, B.N. Datta, Robust partial quadratic eigenvalue assignment with time delay using the receptance and the system matrices, J. Sound Vib. 384 (2016) 1–14.
[18] Z.J. Bai, B.N. Datta, J. Wang, Robust and minimum norm partial quadratic eigenvalue assignment in vibrating systems: a new optimization approach, Mech. Syst. Signal Process. 24 (3) (2010) 766–783.
[19] Z.J. Bai, M.X. Chen, B.N. Datta, Minimum norm partial quadratic eigenvalue assignment with time delay in vibrating structures using the receptance and the system matrices, J. Sound Vib. 332 (4) (2013) 780–794.
[20] R. Storn, K. Price, Differential evolution – a simple and efficient heuristic for global optimization over continuous spaces, J. Global Optim. 11 (4) (1997) 341–359.
[21] R.G. Ghanem, P. Spanos, Stochastic Finite Elements: A Spectral Approach, first ed., Springer, New York, 1991.
[22] M. Eldred, Recent advances in non-intrusive polynomial chaos and stochastic collocation methods for uncertainty analysis and design, in: 50th AIAA/ASME/ASCE/AHS/ASC Structures, Structural Dynamics, and Materials Conference, 2009, pp. 1–37.
[23] B. Sudret, Global sensitivity analysis using polynomial chaos expansions, Reliab. Eng. Syst. Saf. 93 (7) (2008) 964–979.
[24] A. Visioli, Practical PID Control, Advances in Industrial Control, first ed., Springer, New York, 2006.
[25] E. Balmès, Frequency domain identification of structural dynamics using the pole/residue parametrization, in: IMAC XIV - 14th International Modal Analysis Conference – Noise and Vibration Harshness (NVH), 1996, pp. 540–546.